Development 130, 2263-2273

doi:10.1242/dev.00431

DEVELOPMENT AND DISEASE

Mammary gland, limb and yolk sac defects in mice lacking *Tbx3*, the gene mutated in human ulnar mammary syndrome

Todd G. Davenport, Loydie A. Jerome-Majewska and Virginia E. Papaioannou*

Department of Genetics and Development, College of Physicians and Surgeons of Columbia University, 701 W 168th Street, New York, NY 10032, USA

*Author for correspondence (e-mail: vep1@columbia.edu)

Accepted 3 February 2003

SUMMARY

Spontanteous mutations in the T-box gene *TBX3*, result in the human ulnar-mammary syndrome, a dominant developmental disorder characterized by abnormal forelimb and apocrine gland development. In order to develop a mouse model to study the role of this gene during development and disease, we produced a mutation in the mouse ortholog, *Tbx3*. The phenotype of the mutant mice verifies the role of this gene in limb and mammary gland development, and, in addition, reveals a previously unknown role for the gene in the yolk sac, a fetal membrane that is the site of hematopoiesis and is essential for survival during gestation. In homozygous mutant embryos, the yolk sac undergoes cell death and degeneration at midgestation and the fetuses die over a range of several days; none survive to birth. *Tbx3* is the first T-box gene implicated in yolk sac development. Homozygous embryos show a deficiency of mammary gland induction, and exhibit both forelimb and hindlimb abnormalities. Although heterozygous mice, unlike their heterozygous human counterparts, have no apparent phenotype in limb or mammary gland, the homozygous defects in the development of these organs represent more severe manifestations of the defects characteristic of the ulnar-mammary syndrome.

Key words: T-box, Yolk sac, Limb development, *Tbx3*, Ulnar-mammary syndrome, UMS, Mammary gland

INTRODUCTION

Mutations in the human T-box transcription factor gene *TBX3* underlie the autosomal dominant disorder known as ulnar-mammary syndrome (UMS; OMIM 181450) (Bamshad et al., 1997). Human *TBX3* was identified during an attempt to positionally clone the gene responsible for another developmental disorder, Holt-Oram syndrome, which had been mapped to chromosome 12q. Although it was later found that Holt-Oram syndrome is caused by mutations in the closely linked human *TBX5* gene (Basson et al., 1997; Li et al., 1997), mutations in *TBX3* were identified in individuals with ulnar-mammary syndrome, a developmental disorder that was also mapped to this chromosomal region (Bamshad et al., 1995; Bamshad et al., 1997). A number of different mutations in *TBX3* have been identified in families with ulnar-mammary syndrome, most of which are predicted to encode truncated proteins or missense mutations resulting in loss of function (Coll et al., 2002) (for a review, see Papaioannou, 2001). UMS is fully penetrant but with a highly variable clinical presentation, even among family members with the same mutation. As the name suggests, the syndrome is predominately characterized by posterior forelimb deficiencies or duplications, involving the ulna and little finger (with rare involvement of the hindlimb), and apocrine/mammary gland hypoplasia or dysfunction with absent or abnormal nipples. Other common features are abnormal dentition, delayed puberty, genital abnormalities and growth retardation (Bamshad et al., 1995; Bamshad et al., 1999; Bamshad et al., 1996). There have been no reports of humans homozygous for *TBX3* mutations.

TBX3 and the mouse ortholog, *Tbx3*, which was discovered by Bollag et al. (Bollag et al., 1994), are members of the Tbx2 subfamily of the T-box family of transcription factor genes. The family is characterized by a highly conserved sequence encoding a DNA-binding domain, called the T-domain, that binds specific sequences in the promoters of target genes. The Tbx2 subfamily, which includes *Tbx2*, *Tbx3*, *Tbx4* and *Tbx5*, evolved by tandem duplication of an ancestral locus to form a linked pair of genes, followed by duplication of the gene pair and dispersal to two chromosomal locations. In both mouse and human, *Tbx2* and *Tbx4* are linked, and *Tbx3* and *Tbx5* are linked (Agulnik et al., 1996; Papaioannou, 2001). The relatively recent separation of the paralogs, *Tbx2* and *Tbx3*, is reflected in ~90% identity in amino acid sequence in the T-box and similarities in expression patterns and function of the two genes (Agulnik et al., 1996; Brummelkamp et al., 2002; Chapman et al., 1996b; Gibson-Brown et al., 1998a; Gibson-

Brown et al., 1998b; Jacobs et al., 2000; Lingbeek et al., 2002). Both of the mouse genes and their human counterparts can act as transcriptional repressors (Carlson et al., 2001; Carreira et al., 1998; He et al., 1999), and although no downstream target genes have yet been identified for mouse *Tbx3*, the human genes *TBX3* and *TBX2* were both identified in functional screens as negative regulators of the cell cycle control gene *Cdkn2a*. *TBX2* and *TBX3* repress the *Cdkn2a* transcript $p14^{ARF}$ in humans (known as $p19^{ARF}$ in mouse) through an interaction with a variant T-domain binding site that is specific to these two T-box genes (Brummelkamp et al., 2002; Jacobs et al., 2000; Lingbeek et al., 2002). Recently, the crystal structure of TBX3 in complex with DNA has been reported and suggests that TBX3 binds as a monomer to its natural target sites (Coll et al., 2002).

The highly specific patterns of T-box gene expression during development implicate them in many developmental processes (Papaioannou, 1997; Papaioannou, 2001; Smith, 1999). In addition to the UMS mutations in *TBX3*, mutations in several other T-box genes confirm their vital developmental roles in a variety of metazoan species, including human and mouse (Basson et al., 1997; Bruneau et al., 2001; Chapman et al., 1996a; Jerome and Papaioannou, 2001; Russ et al., 2000). In general, the phenotypic abnormalities observed in these mutants correlate with areas of gene expression. In mouse, *Tbx3* is first expressed in the inner cell mass (ICM) of the blastocyst, and later in the mesoderm and endoderm layers of the yolk sac, and in the mesoderm of the amnion, chorion and allantois during gastrulation. During organogenesis, *Tbx3* is expressed in the primordia of many tissues and organs, notably in the apical ectodermal ridge (AER) and the anterior and posterior margins of the developing limbs, and in the epithelium of the mammary buds (Chapman et al., 1996b; Gibson-Brown et al., 1996; Gibson-Brown et al., 1998b; Yamada et al., 2000). *Tbx3* is also expressed in various adult organs (Bollag et al., 1994). Less is known about the spatial pattern of expression in humans, but the gene is expressed in a variety of adult organs, as well as in fetal lung, kidney, heart, liver, spleen and pituitary gland (Bamshad et al., 1999; Bamshad et al., 1997). It has been postulated that the abnormalities seen in individuals with UMS result from a haploinsufficiency of *TBX3* that leads to hypoplasia of tissues through an interference with apoptosis or differentiation during critical stages of embryogenesis (Bamshad et al., 1997; Carlson et al., 2002). To provide a mouse model of UMS in order to understand the developmental role of *Tbx3*, we have generated a mutation in mouse *Tbx3* by gene targeting in embryonic stem cells. In contrast to human UMS mutations, the mouse *Tbx3* mutation is recessive on several genetic backgrounds, with the exception of a mild defect in female genitalia. However, the homozygous mutant phenotype reflects the predominant features of UMS with severe defects in forelimb and mammary gland development and, in addition, reveals a novel role for *Tbx3* in the yolk sac.

MATERIALS AND METHODS

Targeting the *Tbx3* locus

Mouse *Tbx3* genomic clones were isolated from a genomic λ phage 129/SvJ library (Stratagene, La Jolla, CA). The targeting construct, which contains 7.2 kb of total homology was generated by replacing a 3.2 kb *Spe*I fragment containing three coding exons of the T-box with a *lox*P-flanked selection cassette containing the herpes simplex virus thymidine-kinase gene (hsv-tk) under the control of its own promoter and the neomycin-resistance gene under the control of the phosphoglycerate kinase promoter (pgk-neo). The diptheria toxin gene under the control of the β-actin promoter was placed 5′ of the upstream homology for negative selection and the construct was linearized at a unique *Not*I site. The linearized targeting construct (Fig. 1A) was electroporated into R1 ES cells (Nagy et al., 1993) and drug-resistant clones were screened for homologous recombination using Southern blot analysis (Fig. 1A,B). One targeted cell line was recovered and was then transiently transfected with a circular pIC-Cre plasmid (Gu et al., 1993) and grown in media containing FIAU to select for removal of the thymidine kinase gene (Fig. 1A). The targeting strategy deletes three exons encoding 158 amino acids of the T domain and, if splicing were to occur between exons 1 and 4 flanking the deleted region, a frameshift would lead to a premature stop codon at the next codon. Three Cre-excised cell clones were recovered and injected into C57BL/6Tac blastocysts (Taconic Farms, Germantown, NY) to produce chimeras (Papaioannou and Johnson, 2000), which were bred to C57BL/6Tac and 129 mice. Germline transmission of the targeted, Cre-excised allele, $Tbx3^{tm1Pa}$, was obtained from all three cell lines. Subsequent analysis using each of these three lines gave the same range of phenotypes and data from these lines have been combined.

Animals and collection of embryos

Analyses of neonatal and adult heterozygous mice was performed on the following genetic backgrounds: (C57BL/6TacX129)F_1, F_2 and F_2 intercross, and 129 inbred. Analysis of embryos was performed on these backgrounds, as well as on random-bred Swiss-Webster and ICR mice (Taconic Farms, Germantown, NY). Because no differences in phenotype were seen on these different backgrounds, the data have been combined. Heterozygous mice and wild-type littermates were examined for limb and tooth defects, and weighed at 2, 4 and 6 weeks of age. Females were examined for the presence and number of nipples, and the day of vaginal opening was scored. External genitalia were examined at birth, weaning and in adults. Embryos were collected from timed matings (day of the plug=0.5 days post coitus, dpc) and fixed in either Bouin's fixative for histology, or 4% paraformaldehyde for in situ hybridization or immunohistochemistry. Mutant and wild-type embryos, with their yolk sacs and placentae, were histologically examined after Hematoxylin and Eosin staining at 8.5, 10.5, 12.5 and 13.5 dpc. Offspring and embryos were genotyped using a three-primer PCR protocol designed to amplify wild-type and mutant bands using the following primers: (1) 5′-CTAAGCCTGATG-GTGTGAGA-3′; (2) 5′-GATAAACCTCAATGCTACCTAC-3′; and (3) 5′GACTTATCATTCAGCCCAGCAG-3′ (Fig. 1C). PCR conditions were 3 minutes at 94°C, 40 cycles (30 seconds at 94°C, 30 seconds at 59°C, 30 seconds at 72°C), and 10 minutes at 72°C.

In situ hybridization, immunohistochemistry and histology

Whole-mount in situ hybridization was performed as described previously (Wilkinson, 1992). PECAM-1 antibody staining (PharMingen; San Diego, CA) on whole yolk sacs was performed using standard protocols (Davis et al., 1991). Apoptosis was examined in yolk sacs from 9.5 dpc and 10.5 dpc embryos that were living at the time of recovery (two mutant and two wild-type at each age) using immunohistochemistry for activated caspase (Cell Signaling technology, NEB, Beverley, MA) (Di Cunto et al., 2000). For detection of mammary bud induction in homozygous mutant embryos, embryos alive at the time of recovery were examined by in situ hybridization for *Wnt10b* (11.5 and 12.5 dpc) and *Lef1* (12.5 and 13.5 dpc), along with stage and age-matched controls. Embryos (12.5 and 13.5 dpc) were examined histologically in serial sections as described above for evidence of mammary bud development. The following

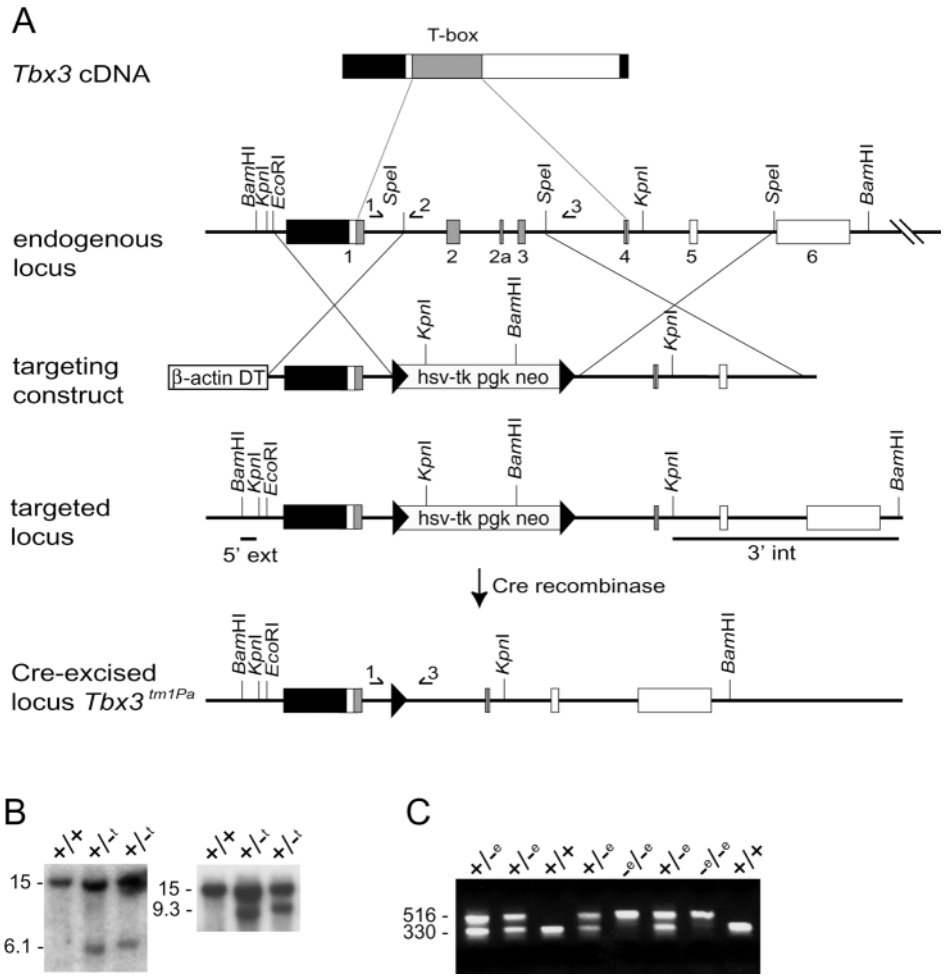

Fig. 1. Targeted disruption of mouse *Tbx3* to produce the *Tbx3*^{tm1Pa} allele by homologous recombination in embryonic stem (ES) cells, followed by in vitro Cre-mediated excision. (A) The *Tbx3* cDNA and exons 1-6 of the endogenous locus are shown. The T-box is shaded, coding exons are shaded or open boxes, the 5′ and 3′ UTR are shown as black boxes, and *lox*P sites are black arrowheads. The targeting construct, containing 7.2 kb of total homology, replaced three coding exons of the T-box with a *lox*P-flanked hsv-tk PGK-neomycin resistance cassette. A β-actin-diptheria toxin (β-actin DT) cassette (Maxwell et al., 1987) was used for negative selection. (B) Southern analysis of *Bam*HI-digested genomic DNA from wild-type and targeted ES cell clones using the 5′ external (ext) and 3′ internal (int) probes indicated in A to distinguish a 15 kb endogenous band (+) from a 6.1 or 9.3 kb targeted band (–^{t}) with the 5′ or 3′ probes, respectively. (C) PCR genotyping of mice using primers indicated in A to distinguish a 330 bp wild-type and a 516 bp mutant band from the Cre-excised allele, *Tbx3*^{tm1Pa} (–^{e}).

markers of limb development were examined by in situ hybridization on mutants and age/stage matched controls: *Shh* (10.5, 11.5 and 12.5 dpc); *Fgf8*, engrailed 1 (*En1*), *Wnt7a* and *Tbx2* (10.5 and 11.5 dpc); *Msx1*, *Tbx4* and *Tbx5* (10.5 dpc); *Hand2* (9.5 and 10.5 dpc).

Adult mammary gland analysis

Inguinal mammary glands were collected from six-week-old virgin females, pregnant females (12.5 days of gestation), lactating females (2 weeks after parturition) and postlactation females (1 week after weaning). The virgin and pregnant females were from both 129 inbred and C57BL/6Tac-129 mixed background mice (F_2 and F_2 intercross), whereas the lactating and postlactation glands were from the mixed background only. Three or four glands were examined from each genotype and background. In each case, the right inguinal mammary gland (number 4) was isolated from the skin by blunt dissection and scraping with a scalpel, and then spread onto a glass slide for overnight fixation in Carnoy's fixative. Fixed glands were stained in Carmine Alum, using standard procedures (Kordon and Smith, 1998). Glands were scored using a semi-quantitative measure for the extent of ductal development and the ratio of terminal end buds to end buds.

Skeletal preparations and measurements

Standard methods were used for Alcian Blue/Alizarin Red skeletal preparations of embryos (Mallo and Brändlin, 1997). For measurements of the posterior zeugopod bones, late fetal stage embryos (17.5 dpc for ulna measurements and 18.5 dpc for fibula measurements) were stained and the limb bones were measured using a grid under a dissecting microscope.

RESULTS

Lack of a major heterozygous effect of the *Tbx3* mutation in mice

Mice heterozygous for the *Tbx3*^{tm1Pa} allele are born at the expected frequency (72/163 from 34 litters of heterozygous × wild type matings; χ^2=2.21, P>0.05), and are viable and fertile. On different genetic backgrounds, no differences were observed in growth rates between heterozygous (n=44) and wild type (n=64) mice (data not shown), in the number and location of nipples in females, or the age of puberty in females, as measured by the day of vaginal opening (average for heterozygotes, 26.3 days, n=21; average for wild type, 25.8 days, n=29; Mann-Whitney U test, z=0.934; P>0.17). Dentition was grossly normal. Skeletal preparations of late fetal stages were carried out for the examination of the bones of the fore- and hindlimbs. The number of digits and digit bones were all normal and there was no fusion of carpal bones, a common feature of UMS. There was no difference in the lengths of the posterior zeugopod elements, the ulna and fibula, between heterozygous and wild-type mice (Table 1).

No difference was seen between wild-type and heterozygous females in the extent of ductal development of the virgin inguinal (number 4) mammary glands (Fig. 2A,B) or in the ratio of end buds to terminal end buds. Pregnant, lactating and

Table 1. Ulna and fibula lengths in *Tbx3* heterozygous (+/–) and wild type (+/+) embryos at late fetal stages in 129 mice and mice of a C57BL/6Tac,129 mixed background

	Genotype							
	+/+		+/–		+/+		+/–	
Background	*n*	Ulna length (mm±se)	*n*	Ulna length (mm±se)	*n*	Fibula length (mm±se)	*n*	Fibula length (mm±se)
Mixed	12	3.75±0.07	18	3.64±0.05		ND		ND
129	4	3.5±0	17	3.5±0	26	3.56±0.16	32	3.55±0.21

ND, not determined.

postlactation involuting inguinal mammary glands were indistinguishable between heterozygous and wild-type females (Fig. 2C,D), and heterozygous mice had no apparent difficulty in nursing and rearing offspring.

The only trait that differentiated *Tbx3* heterozygous from wild-type mice was a minor difference in external genitalia in adult mice. In a sample of 85 heterozygous and 82 wild-type mice from mixed genetic backgrounds, all of the heterozygotes and none of the wild-type females had a small ventral split in the glans clitoris, resulting in a distal bifurcation of the prepuce. In addition, a small proportion of these heterozygous females (9/85) showed a failure of vaginal opening, whereas this was not observed in the wild-type mice.

Embryonic lethality and yolk sac defects in *Tbx3* homozygous mutant mice

No *Tbx3*^{tm1Pa} homozygous mutants were recovered at term in 18 litters from inter se matings of *Tbx3*^{tm1Pa}/+ mice. Examination of embryos during gestation revealed that homozygous mutants were present at the expected Mendelian ratios (Table 2A; χ^2=0.0318, P>0.05), but about half of them (17/35) were dead by 11.5 dpc and none survived beyond about 16.5 dpc (Table 2B). The occasional abnormalities seen in +/+ or *Tbx3*^{tm1Pa}/+ embryos ranged from open brains to a placenta with no embryonic remains, whereas the phenotype of *Tbx3*^{tm1Pa}/*Tbx3*^{tm1Pa} homozygous mutant embryos consists of three major abnormalities: yolk sac defects, lack of mammary glands and limb defects. Prior to the onset of lethality at 10.5 dpc, some homozygous mutant embryos have normal yolk sacs (Fig. 3E,F), but others (6/24) show a reduction in yolk sac vasculature (Fig. 3A). In these mutant embryos, yolk sac blood vessels were small or absent, as confirmed by immunostaining for an endothelial marker, PECAM (Fig. 3B-D), and sometimes contained no detectable blood, although blood was present in the heart and embryonic circulation. At 9.5 and 10.5 dpc, no difference in the amount of apoptosis was detected between mutant and wild-type yolk sacs of living embryos using activated caspase immunohistochemistry (data not shown). By 12.5 dpc, however, most mutant embryos were dead (21/33) and the yolk

Table 2. Genotype and morphology of embryos from matings of *Tbx3*^{tm1Pa}/+ mice

A Proportion of phenotypically abnormal embryos (abnormal/total) of each genotype at different stages of gestation from litters in which all embryos were genotyped

	Genotype		
Age of embryos (dpc)	+/+ (abnormal/total)	*Tbx3*^{tm1Pa} /+ (abnormal/total)	*Tbx3*^{tm1Pa} /*Tbx3*^{tm1Pa} (abnormal/total)
8.5	0/6	0/2	0/5
9.5	1/20	1/18	5/11
10.5	1/7	0/19	7/10
11.5	0/6	1/21	8/8
12.5	2/27	0/55	27/27
16.5	0/6	1/26	9/9
Total number of embryos	72	141	70

B Number of *Tbx3*^{tm1Pa}/*Tbx3*^{tm1Pa} homozygous mutant embryos in different phenotypic categories at different stages of gestation. This table includes all of the homozygous mutant embryos in A, as well as additional mutant embryos

Age of embryos (dpc)	Normal	Abnormal limbs only	Abnormal limbs and yolk sac (live)	Dead* (degenerating)	Total
8.5	5				5
9.5	8†	2		1	11
10.5	3	15	6		24
11.5		15	3	17‡	35
12.5		7	5	21	33
13.5			4	3§	7
14.5-18.5				15¶	15

*Embryos had morphological features indicating death had occurred one or more days previously. Limb morphology could not be assessed in most of these embryos.

†Two of these embryos had open brains.

‡Characteristic limb abnormalities could be seen in two of these embryos.

§Characteristic limb abnormalities could be seen in one of these embryos.

¶Characteristic limb abnormalities could be seen in two of these embryos

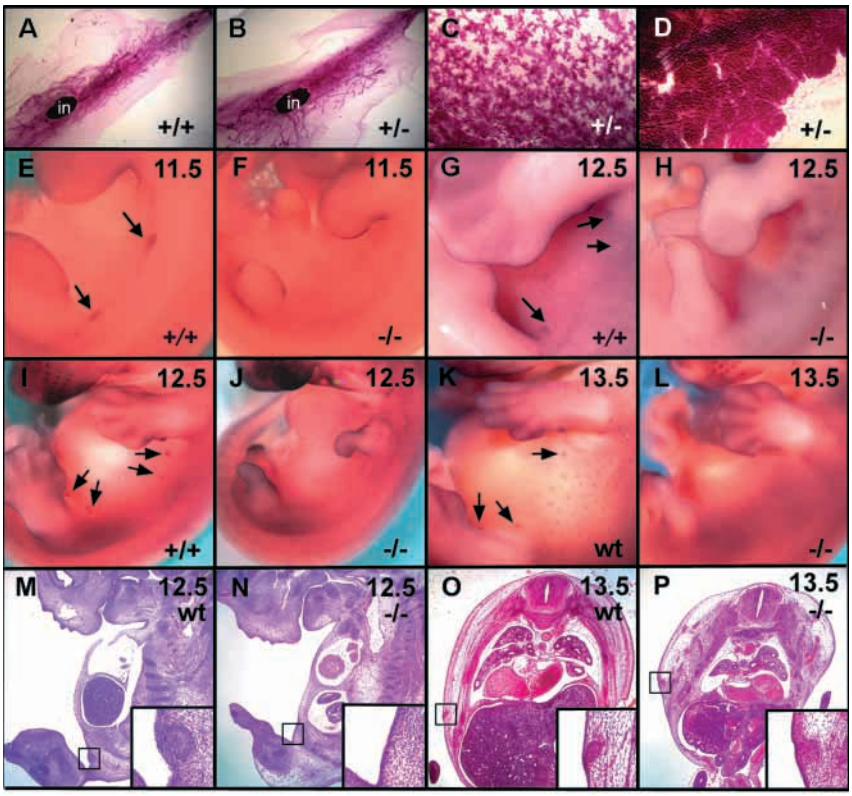

Fig. 2. Mammary gland development in wild type (+/+) and heterozygous *Tbx3*^{tm1Pa} (+/–) adult females and in wild-type (either +/+ or +/–) and *Tbx3*^{tm1Pa}/*Tbx3*^{tm1Pa} (–/–) embryos. (A,B) Wholemounts of the right inguinal mammary glands of 6-week-old virgin females showing a similar extent of duct growth within the fat pad (in, inguinal lymph node). (C,D) Mammary glands from pregnant and lactating heterozygous females, respectively, showing normal ductal growth and lactation that was indistinguishable from controls. (E-H) *Wnt10b* expression in 11.5 and 12.5 dpc embryos. No mammary buds are evident in the mutant embryos (F,H), whereas buds are evident in the wild-type embryos (E,G; arrows). (I-L) *Lef1* expression in 12.5 and 13.5 dpc embryos. No mammary buds are evident in the mutant embryos (J,L), whereas they are clearly visible in the wild-type embryos (I,K; arrows). The development of the forelimb and vibrissae in the 13.5 dpc mutant embryo (L) indicates that it is at a similar developmental stage as the 12.5 dpc control (I). (M-P) Sagittal and transverse sections of 12.5 and 13.5 dpc embryos, respectively. No mammary buds were seen in the 12.5 dpc mutant embryos (N), although three buds out of an expected 20 were seen in two mutant embryos at 13.5 dpc (P). Insets are higher magnification images of the boxed area showing details of the mammary bud region.

sacs of many of the surviving mutants were abnormal. Histologically, the endoderm layer of abnormal-appearing yolk sacs consisted mostly of dead cells with pyknotic nuclei, and the blood vessels had begun to deteriorate (Fig. 3G,H). No obvious abnormalities were seen in placental morphology or morphology of fetal organs and tissues with the exception of a smaller than normal liver (see Fig. 2M-P). No surviving homozygous mutant embryos were observed beyond 13.5 dpc, although two dead fetuses were recovered near term that had survived to about 16 dpc, judging from their developmental stage (Fig. 4E-H).

Failure of mammary gland induction in *Tbx3*^{tm1Pa}/*Tbx3*^{tm1Pa} embryos

Mammary gland development begins with the induction of localized ectodermal placodes along the lateral body wall at 10.5 dpc that results in the formation of discrete, lens-shaped epithelial mammary buds by 12.5 dpc. *Tbx3* expression first begins to appears in the epithelium of the nascent mammary bud at 11.5 dpc and is present in the buds of all male and female embryos between 12.5 and 14.5 dpc (Chapman et al., 1996b) (data not shown). *Tbx3* expression is also seen in adult mammary glands and mammary tumors by Northern analysis (T.G.D. and V.E.P., unpublished). Induction of the mammary bud epithelium was examined in mutant embryos that were still alive at 11.5-13.5 dpc using histology and in situ hybridization for *Wnt10b* and *Lef1*. *Wnt10b* is normally expressed in a raised streak of lateral body wall epithelium at 11.5 dpc, just before the formation of the mammary buds, and then becomes restricted to epithelial mammary buds at 12.5 dpc (Christiansen et al., 1995). *Lef1* is also expressed in the epithelial buds between 11.5 and 13.5 dpc, and is then downregulated (Mailleux et al., 2002). In *Tbx3* mutant embryos, neither *Wnt10b* nor *Lef1* was observed between 11.5 and 13.5 dpc (Fig. 2E-L). This lack of mammary bud induction is not due to a general developmental delay, which is sometimes observed in later stage mutants, as wild-type controls clearly showed evidence of mammary bud induction at comparable developmental stages (e.g. compare Fig. 2I with 2L). Seven 12.5-13.5 dpc mutant embryos were examined histologically in serial sections for evidence of mammary bud induction (Fig. 2M-P). No buds were detected at 12.5 dpc, although at 13.5 dpc one mutant has a single, small pair of mammary buds at the level corresponding to bud number 2, and a second mutant has a single, unilateral bud in a similar position (Fig. 2P). These embryos were somewhat smaller than littermate controls but were judged by the development of the ear pinnae and the vibrissa to be of a comparable developmental stage, appropriate to their chronological age. No cell death was observed within these buds, although they were less well organized than the buds from wild-type embryos (Fig. 2O,P).

Limb abnormalities in *Tbx3*^{tm1Pa}/*Tbx3*^{tm1Pa} embryos

Homozygous mutant embryos are normal at 8.5 dpc, but about 70% of mutants are identifiable by reduced hindlimb bud development by 9.5-10.5 dpc, whereas the forelimb bud appears to be normal in size and shape at this stage. By 11.5 dpc, all homozygous embryos that were alive, or were dead but sufficiently intact to be scored, displayed both fore- and hindlimb abnormalities, with irregularities in the hand plate and either very little development or an irregular shape to the foot plate that resembled a posterior deflection of the autopod (Table 2B; Fig. 4A-D). The AER is present in both fore- and hindlimbs, although it appears reduced in the forelimb and

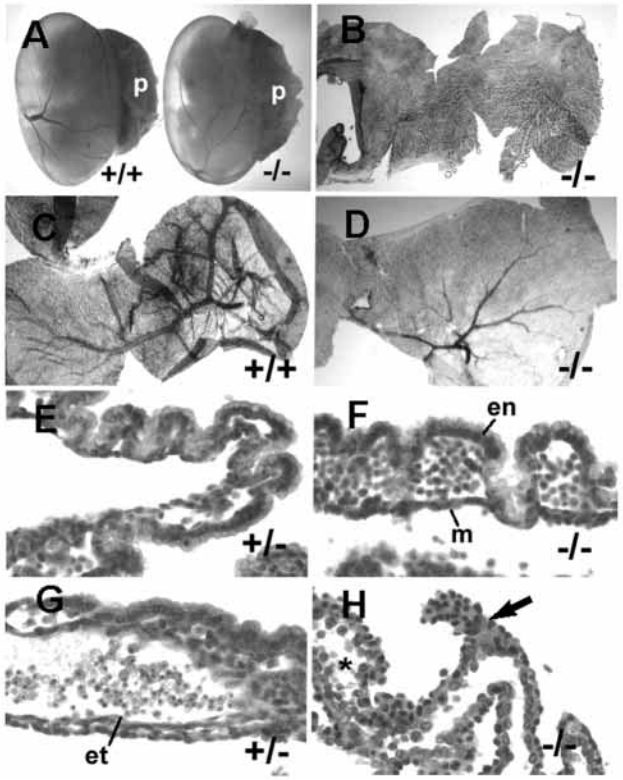

Fig. 3. Yolk sac defects in *Tbx3*^{tm1Pa} mutant mice. (A) 12.5 dpc wild-type (+/+) and homozygous *Tbx3*^{tm1Pa} mutant (–/–) embryos within the yolk sacs, with the placentas (p) still attached. Vasculature is present in the mutant, but the vessels are smaller. (B-D) PECAM immunostaining on dissected yolk sacs at 10.5 dpc showing extensive endothelial cell organization into vessels in the wild-type (C) yolk sac but a variable degree of endothelial development in the homozygous mutants (B,D). (E,F) Histological sections of yolk sacs from heterozygous and homozygous mutant embryos at 10.5 dpc showing normal development of endoderm and mesoderm layers of the yolk sac, and endothelial cell-lined blood islands or blood vessels. (G,H) Histological sections of yolk sacs from heterozygous and homozygous mutant embryos at 12.5 dpc, showing cell death and degeneration of the endoderm layer and blood islands in the homozygous mutant (H). The endoderm cells in the mutant are pyknotic (arrow); asterisk indicates the remains of a vessel or blood island with degenerating blood cells. There were no obvious differences between +/+ and +/– embryos. en, endoderm; et, endothelium; m, mesoderm; p, placenta.

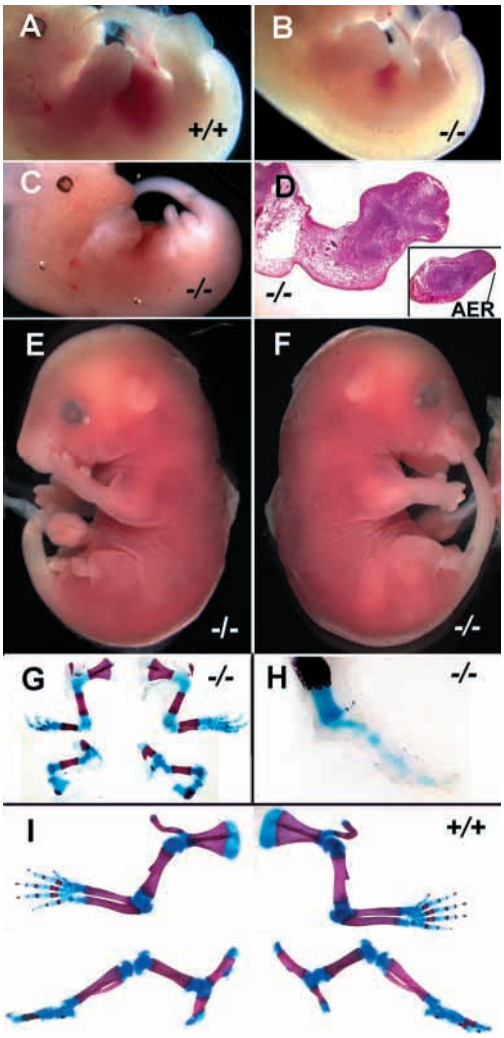

Fig. 4. Limb abnormalities in *Tbx3*^{tm1Pa} homozygous mutant (–/–) mice. (A-C) Limb morphology of 12.5 dpc embryos. The hindlimb of *Tbx3* mutant mice (B,C) is more severely affected than the forelimb, although the phenotype is variable between mice and between contralateral sides of the same mouse. (D) Histology of the forelimb and hindlimb (inset) of a homozygous mutant embryo showing abnormal development of the hand plate and severe truncation of the hindlimb. (E,F) Left and right sides of a homozygous mutant embryo recovered dead near term. (G) Skeletal preparation of limbs from embryo in E,F. The forelimbs exhibit variable abnormalities of the posterior elements, including the ulna and digits, whereas the hindlimb shows severe truncations with a posterior deflection of the zeugopod and no development of the autopod. (H) Right hindlimb of a late term homozygous mutant fetus at higher magnification, showing the single digit attached to the single zeugopod element. (I) Skeletal preparation of the limbs from a normal age-matched control, at the same magnification as G. AER, apical ectodermal ridge.

more severely reduced in the hindlimb as indicated by *Fgf8* expression (Fig. 5A). *Msx1*, which marks cells in the progress zone, was expressed in a normal graded pattern in the fore- and hindlimbs of *Tbx3* homozygous mutant embryos, although the expression in the forelimb appeared to be restricted posteriorly (data not shown). Dorsoventral patterning of the limb is normal, as indicated by the expression of *Wnt7a* in the dorsal ectoderm and engrailed 1 in the ventral ectoderm (data not shown). The expression of two T-box genes implicated in the specification of fore- versus hindlimb, *Tbx5* and *Tbx4*, respectively, is normal (Fig. 5C,D). However, *Tbx2*, a closely related T-box gene with normal expression largely overlapping that of *Tbx3* in the limb bud margins, shows reduced expression in the posterior margin of the forelimb and no expression in the posterior margin of the hindlimb of *Tbx3* homozygous mutants (Fig. 5B). Sonic hedgehog (*Shh*) expression, which marks the zone of polarizing activity (ZPA) at the posterior limb margin, was present in fore- and hindlimbs of three out of four wild-type embryos at 10.5 dpc, and in both limbs of all wild-type embryos at 11.5 dpc. In mutant embryos, however,

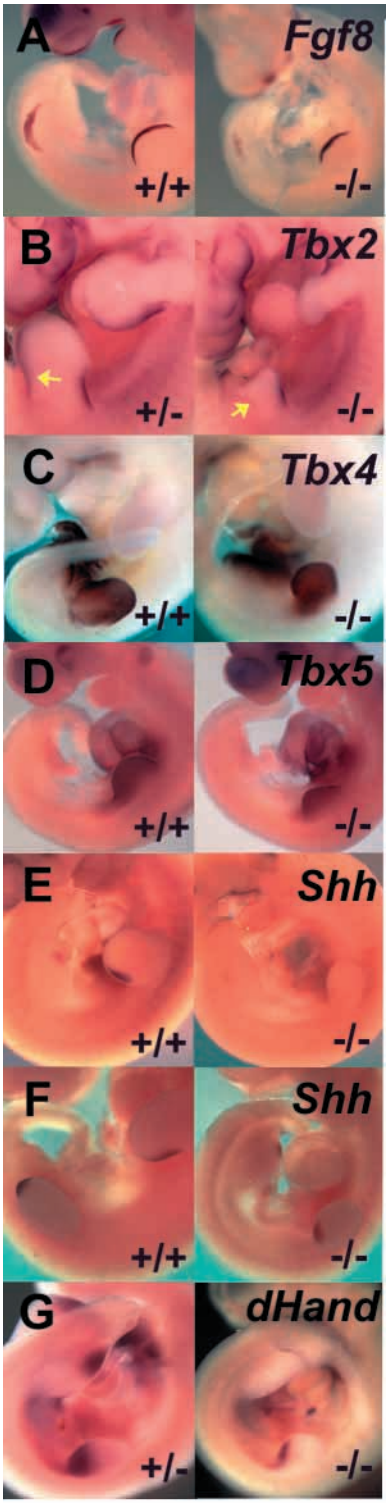

Fig. 5. In situ hybridization showing expression of differentiation and patterning markers in normal (+/+ or +/–) and *Tbx3*^{tm1Pa} homozygous mutant (–/–) embryos. (A) *Fgf8* expression in 10.5 dpc wild-type and homozygous mutant embryos showing the thinner and anteroposteriorly less extensive AER. (B) *Tbx2* expression is absent from the posterior margins of the mutant limbs (arrows indicate posterior margins) but is present at the anterior margin at 11.5 dpc. (C,D) *Tbx4* and *Tbx5* expression in the hind- and forelimbs, respectively, is normal in mutant embryos at 11.5 and 10.5 dpc, respectively. (E,F) *Shh* expression at 10.5 and 11.5 dpc, respectively. Expression is absent or reduced in homozygous mutants compared with wild-type controls. (G) *Hand2* (*dHand*) expression is reduced in the forelimb and absent from the hindlimb of mutant embryos at 10.5 dpc.

there is no expression in stage-matched mutants at 10.5 dpc (Fig. 5E) and only one out of four mutants showed any *Shh* expression at 11.5 dpc. In this embryo, expression was reduced in the forelimbs and limited to a very small area in the hindlimbs (Fig. 5F). *Hand2*, which is initially expressed in the flank and then becomes localized to the posterior limb buds (Charite et al., 2000), is normally expressed in the flank and posterior forelimb bud at 9.5 dpc in mutant and wild-type embryos. However, by 10.5, mutant embryos (n=4) showed a reduced domain of posterior forelimb bud expression compared with stage-matched controls, and none has expression in the hindlimb buds (Fig. 5G).These early limb abnormalities are reflected in corresponding abnormalities of the limb skeleton of the small number of homozygous mutants that reach late fetal stages. In one fetus of ~16.5 dpc (Fig. 4E-G), the right forelimb had a shortened ulna and was missing the metacarpals and phalanges of the fifth digit, and phalanges of the fourth digit. The left forelimb lacked an ulna and carpals as well as metacarpals and phalanges of the fourth and fifth digits (Fig. 4G). In the more severely affected hindlimb, the femur was present, but a single misshapen element represented the zeugopod. A single digit was attached to the zeugopod element of the right hindlimb. In a second fetus of the same approximate age, the right forelimb was shortened but contained an ulna, radius and five digits. The left forelimb was missing the ulna, and the metacarpals and phalanges of the fourth and fifth digits. In the hindlimbs, the femur was present bilaterally; the left hindlimb resembled that of the fetus described above, with a single digit attached to the zeugopodal element; the right hindlimb had a femur, a tibia and a single digit attached to the tibia (Fig. 4H). The pelvic bones were small and poorly formed in both fetuses (Fig. 4G).

DISCUSSION

Differences between UMS and the phenotype of *Tbx3* mutant mice

We have produced a mutation in the mouse T-box gene *Tbx3* that closely corresponds to truncation mutations seen in some individuals with UMS that are predicted to lead to haploinsufficiency through nonsense-mediated mRNA decay (Bamshad et al., 1999). The targeting strategy we used to produce a nonfunctional allele of *Tbx3* deletes three exons encoding most of the DNA-binding T-domain and introduces a frame shift that is predicted to lead to a premature stop codon. If any protein is produced from this allele, it would not be capable of binding DNA (Coll et al., 2002). In spite of this similarity with UMS mutations, however, there are differences in the phenotype of the mutation between human and mouse. First, only a minor heterozygous phenotype is observed in the external genitalia of adult mice, whereas human *TBX3* mutations appear to be completely penetrant with variable expressivity. A spectrum of abnormalities, predominantly in

the forelimb and apocrine glands, but also including abnormal external genitalia such as imperforate hymen, micropenis and imperforate anus, is seen in heterozygous individuals (Bamshad et al., 1999; Bamshad et al., 1996). Second, in human heterozygotes, the forelimb is more frequently and more severely affected than the hindlimb, whereas in homozygous mutant mice, the hindlimb is always the more severely affected limb. Although the phenotype of human *TBX3* mutant homozygotes is unknown, it seems likely that the forelimb will be more severely affected because of the heterozygous phenotype.

Several possibilities could explain these species differences: they could be the result of differences in genetic background modifiers, species-specific differences in dose sensitivity between mice and humans, or alternatively, differences in the developmental role of *Tbx3* between mouse and human. With respect to genetic background effects, humans are generally considered an outbred population and could be segregating for genetic modifiers, which might explain the variable phenotype seen in different individuals with identical *TBX3* mutations. However, in mice with uniform genetic backgrounds (inbred mice and F_1 mice), we have observed variable expressivity. We have also observed a similar variability and range of expressivity in several mixed genetic backgrounds, indicating that phenotypic variability is not due solely to genetic background differences but must also be caused by stochastic events during development. Species differences in dose sensitivity between humans and mice have been observed for a number of other genes [e.g. *SHH* (Chiang et al., 1996; Ming et al., 1998; Roessler et al., 1996) and *PAX9* (Peters et al., 1998; Stockton et al., 2000)], including another T-box gene, *TBX1*, which produces a severe haploinsufficient phenotype in humans that is reflected in a mild and transient heterozygous phenotype in mice (Jerome and Papaioannou, 2001; Lindsay et al., 2001; Merscher et al., 2001). Finally, although it appears that the human mutation is completely penetrant in the pedigrees studied, it could be that other families harbor mutations that go undetected in the heterozygous condition.

The difference in severity between the forelimb and hindlimb is somewhat harder to explain and could represent functional differences in the developmental role of *Tbx3* in limb growth and patterning, or species differences in the expression of *Tbx3* as have been observed between chick and mouse (Gibson-Brown et al., 1998a). *Tbx2* and *Tbx3* are normally expressed in virtually identical patterns in the margins of early limb buds. It is possible that these closely related genes have partially overlapping functions, and that human and mouse have evolved a different balance of function between the two. As yet, no mutations in *Tbx2* have been reported in either species to test this idea. Notwithstanding these species differences, the major aspects of the *Tbx3* mutant phenotype in limb, genitalia and mammary gland in mice correspond to abnormalities characteristic of UMS, and, in addition, a yolk sac defect not reported in humans has been uncovered.

Deficiency of mammary gland induction in *Tbx3* mutant mice

The mammary gland hypoplasia seen in individuals with UMS is reflected in the deficiency in mammary placode induction in homozygous mutant mice and the absence or reduction of mammary buds in mutant embryos. Although there appears to be no haploinsufficiency effect on mammary development or function in heterozygotes, in *Tbx3* homozygous mutant mice, a severe deficiency of mammary development is seen at the earliest stages of mammary bud induction, as indicated by the absence of the two earliest markers of the mammary placode, *Wnt10b* and *Lef1*, and lack of morphological evidence of placodes. Normally, five pairs of mammary placodes form between 11 and 12.5 dpc, but in 13 *Tbx3* homozygous mutants examined either histologically or with molecular probes between 11.5 and 13.5 dpc, only three buds were detected, all of them histologically: one 13.5 dpc embryo had a single, small mammary bud and a second 13.5 dpc embryo had a pair of buds. These embryos were smaller than their normal littermates, but were at comparable developmental stages, as judged by developmental landmarks such as the development of the pinnae of the external ear.

Studies using targeted gene mutations have begun to yield information on the earliest stages of mammary placode induction, and several signaling pathways have been implicated in its control. The five mammary placodes are induced asynchronously between 11 and 12.5 dpc with placode 3 appearing first and placode 2 being the last to form (Mailleux et al., 2002). In addition, induction of the inguinal bud (placode 4) is different from the others in that it is independent of the FGF10/FGFR2 pathway, although its later maintenance depends on FGFR2 activity. Mice with a null mutation of either *Fgf10* or *Fgfr2* develop only the inguinal bud, which is maintained in the absence of FGF10 but not in the absence of FGFR2 (Mailleux et al., 2002). Induction of this inguinal bud also appears to be independent of WNT signaling, as mice lacking LEF1, an effector of WNT/β-catenin signaling, also develop only a single pair of inguinal mammary buds (van Genderen et al., 1994). Mice that lack *Msx2* expression show variable arrest of mammary gland development, but *Msx1*, *Msx2* double homozygotes reveal redundancy for these two transcription factors in early mammary gland induction; placodes form but fail to undergo further development into mammary bud (Satokata et al., 2000), although the status of each individual placode was not reported in this study. The deficiency of mammary placodes in mice lacking *Tbx3* argues that *Tbx3* is required for mammary bud induction and acts upstream of both the FGF and WNT signaling pathway because all of the placodes, including the FGF- and WNT-signaling independent placode 4, are affected. It may be that *Tbx3* is required for mammary epithelium to become competent for continued development, although the rare, late appearance of placode 2 indicates that this requirement is not absolute.

Limb abnormalities in *Tbx3* mutant mice

The deficiency in the development of posterior limb elements in individuals with UMS is reflected in limb abnormalities in mutant mice, including deficiency of the forelimb digits and ulna, as well as the foot and fibula, that result from a failure in the development of posterior limb elements. Limb development and patterning depends on reciprocal interactions between the AER and the ZPA, involving complex signaling through the FGF and SHH signaling pathways (Martin, 2001). FGF signaling from the limb mesenchyme is essential for the formation of the AER, which then induces the ZPA in the

posterior part of the limb. *Shh* signaling from the ZPA is primarily responsible for anteroposterior (AP) patterning of the limb and is regulated by a complex feedback loop with FGFs in the AER (Sun et al., 2000). *Tbx3* is normally expressed both in the AER and in the limb mesenchyme at the anterior and posterior margins of the limbs (Chapman et al., 1996b; Gibson-Brown et al., 1996); therefore, it could be involved in the initiation or maintenance of Fgf gene expression in the AER, and/or *Shh* expression in the ZPA.

The abnormalities in anteroposterior patterning seen in *Tbx3* homozygous mutant limbs closely resemble the limb phenotype seen in mice with homozygous mutations in *Shh*, or with a limb-specific reduction of *Shh* expression (Chiang et al., 2001; Kraus et al., 2001; Lewis et al., 2001), suggesting that *Tbx3* normally functions in the SHH pathway, and that loss or reduction of *Shh* is responsible for the limb phenotype in *Tbx3* mutants. In both *Tbx3* and *Shh* mutants, the posterior tissue of the fore- and hindlimbs is reduced and the AER appears weak and disorganized, as shown by FGF8 expression. In addition, only digit one, a *Shh*-independent digit, forms in the hindlimb of *Tbx3* homozygous mutants.

The similarities in the limb abnormalities observed in *Tbx3* and *Shh* mutant embryos combined with the absence or reduction of *Shh* expression in *Tbx3* homozygous mutants suggest a role for *Tbx3* in the initiation and/or maintenance of *Shh* expression. *Tbx3* is not absolutely required for *Shh* expression because a small proportion of *Tbx3* homozygous mutant embryos express *Shh*, as shown by the presence of *Shh* in one out of four mutants at 11.5 dpc, and by the normally patterned right forelimb in one late stage mutant fetus. We propose that *Tbx3* functions with *Hand2* during early limb patterning to regulate *Shh* expression and set up the initial anteroposterior patterning of the limb. *Shh* expression is then required to maintain and expand the early anteroposterior pattern, and to maintain *Hand2* and *Tbx3* expression in the posterior limb, as the posterior domain of *Tbx3* expression has been shown to be *Shh* dependent (Tumpel et al., 2002).

Alternatively, or in addition to this role in regional signaling in limb patterning, *Tbx3* may play a role in maintaining proliferation in the posterior limb margin. Both *Tbx3* and the closely related *Tbx2* have recently been identified in senescence bypass screens to identify genes that allow the bypass of proliferation arrest (Brummelkamp et al., 2002; Jacobs et al., 2000), implicating these genes in the maintenance of cellular proliferation. A deficiency in the number of posterior limb margin cells in mutants could result in a reduced ZPA, with fewer cells producing SHH. The feedback loop maintaining the AER would consequently be affected. The posterior reduction in *Msx1* expression, which is an AER-independent marker of the progress zone, would fit with a reduction in posterior tissue. Whether the lower expression of *Tbx2* in the posterior margins of the limbs of mutant mice is due to loss of posterior tissue or an interaction between *Tbx2* and *Tbx3* has yet to be determined. This decrease in posterior *Tbx2* expression could also be a direct result of decreased *Shh* expression, as it has been shown that *Shh* can regulate *Tbx2* (Gibson-Brown et al., 1998a).

Embryonic lethality of *Tbx3* homozygous mutants

No homozygous *TBX3* humans have been reported. Our mouse model provides a tentative explanation for this in that the yolk sac, which is vital for hematopoiesis and maternal-fetal exchange during gestation, is severely compromised in mutant mice. Although the yolk sac vasculature initially forms normally in the majority of mutant embryos and blood is produced, massive cell death of the yolk sac endoderm occurs at a variable time during gestation, even though *Tbx3* expression in the yolk sac and other fetal membranes appears to be transitory in the early stages of yolk sac development (Chapman et al., 1996b). In the absence of the detection of other life-threatening abnormalities in fetal membranes or in the fetus, and because some embryos still have a beating heart at the same time as the yolk sac defects are evident, we attribute embryonic lethality to the yolk sac failure, which includes, but is not limited to the vasculature. If there is a similar role for *TBX3* in human fetuses, they too would be lost during gestation. At present, we have no explanation for the variable time of death or the variable expressivity of the yolk sac phenotype, and it is not clear what developmental pathways are affected. It is possible that some mutant embryos survive with a threshold level of yolk sac development only to succumb to delayed effects of an earlier deficiency in the metabolic function of the yolk sac or deficiencies in the vasculature, blood islands or hematopoietic precursors. The small size of the liver in mutant embryos might be a reflection of this deficiency.

The putative function of *Tbx3* in the $p19^{ARF}$/Mdm2/p53 pathway (Brummelkamp et al., 2002; Carlson et al., 2002; Jacobs et al., 2000; Lingbeek et al., 2002) offers a possible explanation for the cell death observed in the yolk sac, as well as the hypoplasia of the mammary bud and posterior limb elements. The failure of *Tbx3* to suppress $p19^{ARF}$ expression in these areas of *Tbx3* embryonic expression could lead to the upregulation of this gene and the subsequent upregulation of *p53*. This in turn could lead to cessation of proliferation and/or increased apoptosis in the yolk sac and eventual death of the fetus. This possibility is under investigation.

In summary, the homozygous *Tbx3* mutant mouse recapitulates two of the major features of UMS, the posterior limb defect and mammary gland hypoplasia, as well as uncovering an additional role for the gene in the yolk sac. *Tbx3* mutant mice provide a means of investigating the involvement of this gene in specific signaling pathways during development of the yolk sac, limb and mammary gland.

We thank V. Aita, D. Chapman, T. Bestor and members of the Papaioannou laboratory for helpful discussion; P. Rodriguez and U. Saha for technical assistance; J. Gao for performing the fibula measurements; B. Hogan and J. Gearhart for mouse embryo cDNA libraries; and R. Axel, R. Grosschedl, A. Joyner, R. Maas, G. Martin, A. McMahon, G. Shackelford and D. Srivastava for generously supplying in situ hybridization probes. This work was funded by a grants from the NIH (RO1 HD33082) and the United States Army Medical Research and Materiel Command Breast Cancer Program (DAMD17-96-1-6090).

REFERENCES

Agulnik, S. I., Garvey, N., Hancock, S., Ruvinsky, I., Chapman, D. L., Agulnik, I., Bollag, R., Papaioannou, V. and Silver, L. M. (1996). Evolution of mouse *T-box* genes by tandem duplication and cluster dispersion. *Genetics* **144**, 249-254.

Bamshad, M., Krakowiak, P. A., Watkins, W. S., Root, S., Carey, J. C. and

Jorde, L. B. (1995). A gene for ulnar-mammary syndrome maps to 12q23-q24.1. *Hum. Mol. Genet.* **4**, 1973-1977.

Bamshad, M., Root, S. and Carey, J. C. (1996). Clinical analysis of a large kindred with the Pallister ulnar-mammary syndrome. *Am. J. Med. Genet.* **65**, 325-331.

Bamshad, M., Lin, R. C., Law, D. J., Watkins, W. S., Krakowiak, P. A., Moore, M. E., Franceschini, B., Lala, R., Holmes, L. B., Gebuhr, T. C. et al. (1997). Mutations in human *TBX3* alter limb, apocrine and genital development in ulnar-mammary syndrome. *Nat. Genet.* **16**, 311-315.

Bamshad, M., Le, T., Watkins, W. S., Dixon, M. E., Kramer, B. E., Roeder, A. D., Carey, J. C., Root, S., Schinzel, A., van Maldergem, L. et al. (1999). The spectrum of mutations in *TBX3*: genotype/phenotype relationship in ulnar-mammary syndrome. *Am. J. Hum. Genet.* **64**, 1550-1562.

Basson, C. T., Bachinsky, D. R., Lin, R. C., Levi, T., Elkins, J. A., Soults, J., Grayzel, D., Kroumpousou, K., Traill, T. A., Leblanc-Straceski, J. et al. (1997). Mutations in human cause limb and cardiac malformations in Holt-Oram syndrome. *Nat. Genet.* **15**, 30-35.

Bollag, R. J., Siegfried, Z., Cebra-Thomas, J. A., Garvey, N., Davison, E. M. and Silver, L. M. (1994). An ancient family of embryonically expressed mouse genes sharing a conserved protein motif with the *T* locus. *Nat. Genet.* **7**, 383-389.

Brummelkamp, T. R., Kortlever, R. M., Lingbeek, M., Trettel, F., MacDonald, M. E., van Lohuizen, M. and Bernards, R. (2002). *TBX-3*, the gene mutated in ulnar-mammary syndrome, is a negative regulator of $p19^{ARF}$ and inhibits senescence. *J. Biol. Chem.* **277**, 6567-6572.

Bruneau, B. G., Nemer, G., Schmitt, J. P., Charron, F., Robitaille, L., Caron, S., Conner, D. A., Gessler, M., Nemer, M., Seidman, C. E. et al. (2001). A murine model of Holt-Oram syndrome defines roles of the T-box transcription factor Tbx5 in cardiogenesis and disease. *Cell* **106**, 709-721.

Carlson, H., Ota, S., Campbell, C. E. and Hurlin, P. J. (2001). A dominant repression domain in Tbx3 mediates transcriptional repression and cell immortalization: relevance to mutations in Tbx3 that cause ulnar-mammary syndrome. *Hum. Mol. Genet.* **10**, 2403-2413.

Carlson, H., Ota, S., Song, Y., Chen, Y. and Hurlin, P. J. (2002). Tbx3 impinges on the p53 pathway to suppress apoptosis, facilitate cell transformation and block myogenic differentiation. *Oncogene* **21**, 3827-3835.

Carreira, S., Dexter, T. J., Yavuzer, U., Easty, D. J. and Goding, C. R. (1998). Brachyury-related transcription factor Tbx2 and repression of the melanocyte-specific TRP-1 promoter. *Mol. Cell. Biol.* **18**, 5099-5108.

Chapman, D. L., Agulnik, I., Hancock, S., Silver, L. M. and Papaioannou, V. E. (1996a). *Tbx6*, a mouse T-box gene implicated in paraxial mesoderm formation at gastrulation. *Dev. Biol.* **180**, 534-542.

Chapman, D. L., Garvey, N., Hancock, S., Alexiou, M., Agulnik, S., Gibson Brown, J. J., Cebra-Thomas, J., Bollag, R. J., Silver, L. M. and Papaioannou, V. E. (1996b). Expression of the T-box family genes, *Tbx1-Tbx5*, during early mouse development. *Dev. Dyn.* **206**, 379-390.

Charite, J., McFadden, D. G. and Olson, E. N. (2000). The bHLH transcription factor dHAND controls *Sonic hedgehog* expression and establishment of the zone of polarizing activity during limb development. *Development* **127**, 2461-2470.

Chiang, C., Litingtung, Y., Lee, E., Young, K. E., Corden, J. L., Wesphal, H. and Beachy, P. A. (1996). Cyclopia and defective axial patterning in mice lacking Sonic Hedgehog gene function. *Nature* **383**, 407-413.

Chiang, C., Litingtung, Y., Harris, M. P., Simandl, B. K., Li, Y., Beachy, P. A. and Fallon, J. F. (2001). Manifestation of the limb prepattern:Limb development in the absence of sonid hedgehog function. *Dev. Biol.* **236**, 421-435.

Christiansen, J. H., Dennis, C. L., Wicking, C. A., Monkley, S. J., Wilkinson, D. G. and Wainwright, B. J. (1995). Murine *Wnt-11* and *Wnt-12* have temporally and spatially restricted expression patterns during embryonic development. *Mech. Dev.* **51**, 341-350.

Coll, M., Seidman, J. G. and Muller, C. W. (2002). Structure of the DNA-bound T-box domain of human TBX3, a transcription factor responsible for ulnar-mammary syndrome. *Structure* **10**, 343-356.

Davis, C. A., Holmyard, D. P., Millen, K. J. and Joyner, A. L. (1991). Examining pattern formation in mouse, chicken and frog embryos with an *En*-specific antiserum. *Development* **111**, 287-298.

Di Cunto, F., Imarisio, S., Hirsch, E., Broccoli, V., Bulfone, A., Migheli, A., Atzori, C., Turco, E., Triolo, R., Dotto, G. P. et al. (2000). Defective neurogenesis in citron kinase knockout mice by altered cytokinesis and massive apoptosis. *Neuron* **28**, 115-127.

Gibson-Brown, J. J., Agulnik, S. I., Chapman, D. L., Alexiou, M., Garvey, N., Silver, L. M. and Papaioannou, V. E. (1996). Evidence of a role for T-box genes in the evolution of limb morphogenesis and the specification of forelimb/hindlimb identity. *Mech. Dev.* **56**, 93-101.

Gibson-Brown, J. J., Agulnik, S. I., Silver, L. M., Niswander, L. and Papaioannou, V. E. (1998a). Involvement of T-box genes *Tbx2-Tbx5* in vertebrate limb specification and development. *Development* **125**, 2499-2509.

Gibson-Brown, J. J., Agulnik, S. I., Silver, L. M. and Papaioannou, V. E. (1998b). Expression of T-box genes *Tbx2-Tbx5* during chick organogenesis. *Mech. Dev.* **74**, 165-169.

Gu, H., Zou, Y. R. and Rajewsky, K. (1993). Independent control of immunoglobulin switch recombination at individual switch regions evidenced through Cre-*loxP*-mediated gene targeting. *Cell* **73**, 1155-1164.

He, M.-L., Wen, L., Campbell, C. E., Wu, J. Y. and Rao, Y. (1999). Transcription repression by *Xenopus* ET and its human ortholog TBX3, a gene involved in ulnar-mammary syndrome. *Proc. Natl. Acad. Sci. USA* **96**, 10212-10217.

Jacobs, J. J. L., Keblusek, P., Robanus-Maandag, E., Kristel, P., Lingbeek, M., Nederlof, P. M., van Welsem, T., van de Vijver, M. J., Koh, E. Y., Daley, G. Q. and van Lohuizen, M. (2000). Senescence bypass screen identifies *TBX2*, which represses *Cdkn2a* ($p19^{ARF}$) and is amplified in a subset of human breast cancers. *Nat. Genet.* **26**, 291-299.

Jerome, L. A. and Papaioannou, V. E. (2001). DiGeorge syndrome phenotype in mice mutant for the T-box gene, *Tbx1*. *Nat. Genet.* **27**, 286-291.

Kordon, E. C. and Smith, G. H. (1998). An entire functional mammary gland may comprise the progeny from a single cell. *Development* **125**, 1921-1930.

Kraus, P., Fraidenraich, D. and Loomis, C. A. (2001). Some distal limb structures develop in mice lacking Sonic hedgehog signaling. *Mech. Dev.* **100**, 45-58.

Lewis, P. M., Dunn, M. P., McMahon, J. A., Logan, M., Martin, J. F., St-Jacques, B. and McMahon, A. (2001). Cholesterol modification of sonic hedgehog is required for long-range signaling activity and effective modulation of signaling by Ptc1. *Cell* **105**, 599-612.

Li, Q. Y., Newbury-Ecob, R. A., Terrett, J. A., Wilson, D. I., Curtis, A. R. J., Yi, C. H., Gebuhr, T., Bullen, P. J., Robson, S. C., Strachan, T. et al. (1997). Holt-Oram syndrome is caused by mutations in *TBX5*, a member of the *Brachyury (T)* gene family. *Nat. Genet.* **15**, 21-29.

Lindsay, E. A., Vitelli, F., Su, H., Morishima, M., Huynh, T., Pramparo, T., Jurecic, V., Ogunrinu, G., Sutherland, H. F., Scambler, P. J. et al. (2001). *Tbx1* haploinsufficiency in the DiGeroge syndrome region causes aortic arch defects in mice. *Nature* **410**, 97-101.

Lingbeek, M. E., Jacobs, J. J. L. and van Lohuizen, M. (2002). The T-box repressors *TBX2* and *TBX3* specifically regulate the tumor-suppressor $p14^{ARF}$ via a variant T-site in the initiator. *J. Biol. Chem.* **277**, 26120-26127.

Mailleux, A. A., Spencer-Dene, B., Dillon, C., Ndiaye, D., Savona-Baron, C., Itoh, N., Kato, S., Dickson, C., Thiery, J. P. and Bellusci, S. (2002). Role of FGF10/FGFR2b signaling during mammary gland development in the mouse embryo. *Development* **129**, 53-60.

Mallo, M. and Brändlin, I. (1997). Segmental identity can change independently in the hindbrain and rhombencephalic neural crest. *Dev. Dyn.* **210**, 146-156.

Martin, G. (2001). Making a vertebrate limb: new players enter from the wings. *BioEssays* **23**, 865-868.

Maxwell, F., Maxwell, I. H. and Glode, L. M. (1987). Cloning, sequence determination, and expression in transfected cells of the coding sequence for the *tox* 176 attenuated diphtheria toxin A chain. *Mol. Cell. Biol.* **7**, 1576-1579.

Merscher, S., Funke, B., Epstein, J. A., Heyer, J., Puech, A., Lu, M. M., Xavier, R. J., Demay, M. B., Russell, R. G., Factor, S. et al. (2001). *TBX1* is responsible for cardiovascular defects in velo-cardio-facial/DiGeroge syndrome. *Cell* **104**, 619-629.

Ming, J. E., Roessler, E. and Muenke, M. (1998). Human developmental disorders and the Sonic hedgehog pathway. *Mol. Med. Today* **4**, 343-349.

Nagy, A., Rossant, J., Nagy, R., Abramow-Newerly, W. and Roder, J. (1993). Derivation of completely cell culture-derived mice from early-passage embryonic stem cells. *Proc. Natl. Acad. Sci. USA* **90**, 8424-8428.

Papaioannou, V. E. (1997). T-box family reunion. *Trends Genet.* **13**, 212-213.

Papaioannou, V. E. (2001). T-box genes in development: from hydra to humans. *Int. Rev. Cytol.* **207**, 1-70.

Papaioannou, V. E. and Johnson, R. (2000). Production of chimeras by blastocyst and morula injection of targeted ES cells. In *Gene Targeting, A Practical Approach* (ed. A. L. Joyner), pp. 133-175. Oxford: Oxford University Press.

Peters, H., Neubuser, A., Kratochwil, K. and Balling, R. (1998). Pax9-deficient mice lack pharyngeal pouch derivatives and teeth and exhibit craniofacial and limb abnormalities. *Genes Dev.* **12**, 2735-2747.

Roessler, E., Belloni, E., Gaudenz, K., Jay, P., Berta, P., Scherer, S. W., Tsui, L. C. and Muenke, M. (1996). Mutations in the human Sonic Hedgehog gene cause holoprosencephaly. *Nat. Genet.* **14**, 357-360.

Russ, A. P., Wattler, S., Colledge, W. H., Aparicio, S. A. J. R., Carlton, M. B. L., Pearce, J. J., Barton, S. C., Surani, M. A., Ryan, K., Nehls, M. C. et al. (2000). *Eomesodermin* is required for mouse trophoblast development and mesoderm formation. *Nature* **404**, 95-98.

Satokata, I., Ma, L., Ohshima, H., Bei, M., Woo, I., Nishizawa, K., Maeda, T., Takano, Y., Uchiyama, M., Heaney, S. et al. (2000). *Msx2* deficiency in mice causes pleiotropic defects in bone growth and ectodermal organ formation. *Nature Genet.* **24**, 391-395.

Smith, J. C. (1999). T-box genes-what they do and how they do it. *Trends Genet.* **15**, 154-158.

Stockton, D. W., Das, P., Goldenberg, M., D'Souza, R. M. and Patel, P. I. (2000). Mutation of PAX9 is associated with oligodontia. *Nat. Genet.* **24**, 18-19.

Sun, X., Lewandoski, M., Meyers, E. N., Liu, Y.-H., Maxson, R. E. J. and Martin, G. R. (2000). Conditional inactivation of *Fgf4* reveals complexity of signalling during limb bud development. *Nature Genet.* **25**, 83-86.

Tumpel, S., Sanz-Ezquerro, J. J., Isaac, A., Eblaghie, M. C., Dobson, J. and Tickle, C. (2002). Regulation of *Tbx3* expression by anteroposterior signalling in vertebrate limb development. *Dev. Biol.* **250**, 251-262.

van Genderen, C., Okamura, R. M., Farinas, I., Quo, R. G., Parslow, T. G., Bruhn, L. and Grosschedl, R. (1994). Development of several organs that require inductive epithelial-mesenchymal interactions is impaired in LEF-1 deficient mice. *Genes Dev.* **8**, 2691-2703.

Wilkinson, D. G. (1992). *Whole Mount In Situ Hybridization of Vertebrate Embryos*. Oxford: IRL Press.

Yamada, M., Revelli, J.-P., Eichele, G., Barron, M. and Schwartz, R. J. (2000). Expression of chick *Tbx-2*, *Tbx-3*, and *Tbx-5* genes during early heart development: Evidence for BMP2 induction of *Tbx2*. *Dev. Biol.* **228**, 95-105.